Heliyon 9 (2023) e16247

Contents lists available at ScienceDirect

Heliyon

journal homepage: www.cell.com/heliyon

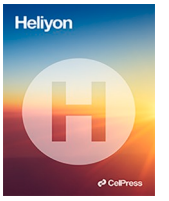

Research article

Insight into the mechanisms of therapeutic hypothermia for asphyxia cardiac arrest using a comprehensive approach of GC-MS/MS and UPLC-Q-TOF-MS/MS based on serum metabolomics

Yiyuan Zhang [a,1], Yang Feng [a,b,1], Fang Chen [c], Jiang Yu [c], Xiehong Liu [c], Yanjuan Liu [c], Jielin Ouyang [a,b], Mingyu Liang [a,b], Yiming Zhu [c,**], Lianhong Zou [a,*]

[a] *The First Affiliated Hospital of Hunan Normal University, Hunan Provincial Key Laboratory of Molecular Epidemiology, Changsha, Hunan, China*
[b] *Department of Emergency Medicine, Hunan Provincial People's Hospital, The First Affiliated Hospital of Hunan Normal University, Changsha, Hunan, China*
[c] *Hunan Provincial People's Hospital, Hunan Provincial Key Laboratory of Emergency and Critical Care Metabolomics,Changsha, Hunan, China*

ARTICLE INFO

Keywords:
Cardiac arrest
Metabolomics
UPLC-Q-TOF-MS/MS
GC-MS/MS
Hypothermia

ABSTRACT

Cardiac arrest (CA) is a severe worldwide health problem. Therapeutic hypothermia is widely used to reduce the cardiac injury and improve the neurological outcomes after CA. However, a few studies have reported the changes of serum metabolic characteristics after CA. The healthy male New Zealand Rabbits successfully resuscitated from 10-min asphyxia-induced CA were divided randomly into the normothermia (NT) group and mild therapeutic hypothermia (HT) group. The sham group underwent sham-operation. Survival was recorded and neurological deficit score (NDS) was assessed. The serum non-targeted metabolomics were detected using ultra-high-performance liquid chromatography-quadrupole time-of-flight tandem mass spectrometry (UPLC-Q-TOF-MS/MS) and gas chromatography tandem mass spectrometry (GC-MS/MS) at 15 min, 3 h, 6 h and 24 h after return of spontaneous circulation (ROSC). Our study showed that the heart rate (HR) significantly slowed down during 0.5–6 h post ROSC, consistent with the decreasing trend of body temperature in the HT group. Compared with the NT group, the levels of Lac and PCO2 at 24 h post ROSC were lower, while a significant increase in PO2 level at 24 h post ROSC was observed in the HT group. The survival rate of the HT group was significantly higher than that of the NT group, and NDS scores were remarkably increased at 24 h post ROSC in the NT group. Significant differences in metabolic profiles at 15 min, 3 h, 6 h and 24 h post ROSC were observed among the Sham, NT and HT groups. The differential metabolites detected by UPLC-Q-TOF-MS/MS and GC-MS/MS were screened for further study between every two groups (NT vs sham, HT vs sham and HT vs NT) at 15 min, 3 h, 6 h and 24 h post ROSC. Phenylalanine metabolism, alanine, aspartate and glutamate metabolism and tricarboxylic acid (TCA) cycle were enriched in NT vs sham, HT vs sham and HT vs NT respectively. Our study demonstrated

* Corresponding author. Department of Emergency Medicine, Hunan Provincial People's Hospital, the First Affiliated Hospital of Hunan Normal University, 61 Jiefang West Road, Changsha, Hunan 410005, PR China.
** Corresponding author. , Hunan Provincial Key Laboratory of Emergency and Critical Care Metabolomics, Hunan Provincial People's Hospital, the First Affiliated Hospital of Hunan Normal University, 61 Jiefang West Road, Changsha, Hunan 410005, PR China.
E-mail addresses: zhuyiming_02@163.com (Y. Zhu), zoulh1986@hunnu.edu.cn (L. Zou).
[1] These authors contributed equally: Yiyuan Zhang, Yang Feng.

https://doi.org/10.1016/j.heliyon.2023.e16247
Received 26 September 2022; Received in revised form 8 May 2023; Accepted 10 May 2023
Available online 19 May 2023
2405-8440/© 2023 The Authors. Published by Elsevier Ltd. This is an open access article under the CC BY-NC-ND license (http://creativecommons.org/licenses/by-nc-nd/4.0/).

that therapeutic hypothermia improves the survival and neurological outcomes in rabbit model of cardiac arrest, and firstly represents the dynamic metabolic changes in the hypothermia therapy for CA by comprehensive UPLC-Q-TOF-MS/MS- and GC-MS/MS-based metabolomics.

1. Introduction

Sudden cardiac arrest (SAD) is one of the major causes of death and disability around the world, while approximately 420,000 people suffering cardiac arrest annually in the United States [1]. At present, the overall survival rate of discharged patients with in-hospital cardiac arrest (IHCA) is between 3% and 27%, while patients with out of hospital cardiac arrest (OHCA) are only 6.4% [2,3]. As a serious public health problem worldwide, most CA patients with ROSC experience a comatose state. Neurologic injury is the leading cause of death in CA patients. Some CA survivors are accompanied by permanent neurological defects. As many as 68% of OHCA and 23% of IHCA patients die from neurologic injury [4]. The poor neurological outcome after resuscitation from cardiac arrest is significantly associated with global cerebral ischemia/reperfusion injury [5].

Targeted temperature management (TTM), previously known as therapeutic hypothermia, which reduces the core temperature to 32–36 °C, is a clinical therapy proven to have neuroprotective benefits and improve survival after ischemic stroke and cardiac arrest [6]. Moreover, the therapeutic hypothermia, the only proven effective treatment, has been incorporated into the guidelines for routine post-resuscitation care and remains a subject of significant controversies in clinical practice. CA patients with ROSC should be treated with therapeutic hypothemia as soon as possible because it has been shown that the beneficial effects of therapeutic hypothermia are time-dependent [7]. An increasing number of research suggests that therapeutic hypothermia decreases or mitigates brain metabolism, inflammatory response, excitotoxicity, intracranial pressure, blood brain barrier disruption and many other factors [8,9]. Understanding the mechanism will be useful in guiding the clinical applications of therapeutic hypothermia and improving its therapeutic efficacy.

Metabolomics is emerging as a powerful platform for reflecting a comprehensive overview of metabolic changes in a complex biological system [10]. A series of analytical platforms have been widely used in detecting the metabolism of organisms, including nuclear magnetic resonance (NMR) spectroscopy, GC-MS/MS and UPLC-Q-TOF-MS/MS [11–13]. Among these high-throughput technologies, the most widely-used is GC-MS/MS and UPLC-Q-TOF-MS/MS, owning the high sensitivity and wide range of detection. Moreover, a single platform is unable to cover the entire metabolites present in a biological sample [14]. Therefore, GC-MS/MS and UPLC-Q-TOF-MS/MS techniques are often used together to improve coverage, accuracy and sensitivity of the identification.

In this study, we demonstrated the mild hypothermia improved the survival and neurological outcomes in rabbits with CA. In addition, we performed GC-MS/MS and UPLC-Q-TOF-MS/MS based serum metabolomics to identify the dynamic changes in metabolism and potential pathophysiological implications in CA rabbits with or without therapeutic hypothermia treatment. Collectively, our results provide novel insights into the protective mechanism of therapeutic hypothermia for CA from the perspective of metabolomics.

2. Metarials and methods

2.1. Animals and groups

Twenty-six healthy New Zealand male rabbits weighing 2.5 kg were obtained from Hunan Slac Jingda Laboratory Animal Company Ltd. (Changsha, China; license No. SCXK (Xiang)2013–0004). The animals were randomly divided into three groups: sham operation (sham, n = 6), normothemia treatment (NT, n = 10) and hypothermia treatment (HT, n = 10). Rabbits were kept in standard condition at 37 °C ± 0.5 °C and 70% humidity for a week. We followed the guideline for ethical review of animal welfare of China (GB/T 35,892–2018), and all experiments were obtained an approval from with the Medical Ethics Review Committee of Hunan Provincial People's Hospital (approval No.20190218175).

2.2. Asphyxial CA model of rabbit

The rabbits were fasted for 12 h except for water, and then were anesthetized with 3% pentobarbital (30 mg/kg). Animals were fixed and monitored systemic mean arterial pressure (MAP), HR and electrocardiogram (ECG) using BL-420 S Biological Function Recording system. The body temperature was measured using a commercial rectal temperature sensor. Sham animals underwent only general anesthesia and endotracheal intubation.

Cardiac arrest was induced by asphyxia. The criterion of CA was no activity in the ECG signal and the MAP <10 mmHg. Animals were mechanically ventilated with a ventilator (tidal volume, 20 ml/kg; respiratory rate, 50 breaths/min; inspiratory-to-expiratory ratio, 4:5) and chest compressions (180 beats/min) with injection of epinephrine (0.02 mg/kg) after 10 min of asphyxia induced CA (Total duration of hypoxia was 10 min). The successful ROSC criterion was MAP >60 mmHg for a minimum of 10 min and autonomic respiration. Animals in the NT group were maintained at the normal body temperature of 37 ± 0.5 C during the treatment [15,16].

In the HT group, the objective temperature of rabbits was 32 ± 0.5 C and needed to be cool quickly. Briefly, ice packs were frozen at −20 °C overnight and applied under the operating table immediately after ROSC. Animals were maintained in this mild hypothermia

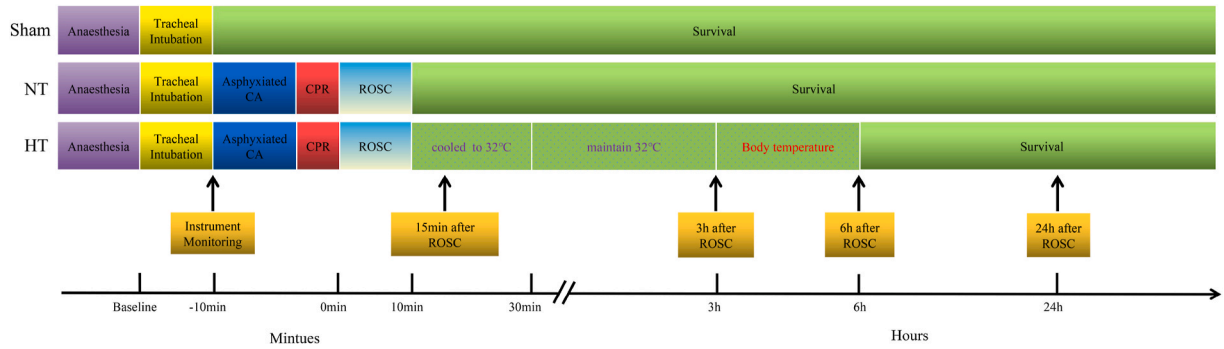

Fig. 1. The experimental workflow in the sham group, the NT group and the HT group.

status for 3 h and with a continuously monitored body temperature maintained at 32°C–35 °C [17]. Subsequently, the body temperature of the mild hypothermia rabbits will return to normal through increasing the environment temperature using an electric blanket. The experimental schematic for asphyxial cardiac arrest is shown in Fig. 1.

2.3. Serum sample collection

The blood were collected from 26 rabbits including sham group (n = 6), NT group (n = 10), HT group (n = 10) at various time points (at 15 min, 3 h, 6 h and 24 h) post ROSC. Then, the blood samples were centrifuged (3000 rpm, 5 min) to obtain the serum. Serum was transferred to a clean Eppendorf (EP) tube and subsequently stored at −80 °C.

2.4. Neurological assessment and survival rate

NDS at 24 h post ROSC were evaluated using the Neurological Deficit Grading Scale by three investigators under double-blinded conditions (0–10% normal, 100% brain death). Meanwhile, all rabbits without treatments had been evaluated to ensure normal neurological function [18,19]. The survival of cardiac arrerst rabbits was recorded during 10 days after ROSC. Then, the survival curve was conducted to evaluate the protective effect of therapeutic hypothermia on cardiac arrest.

2.5. Blood-GAS analysis

Due to the rabbit sham group were not treated with CA, we collected blood extraction via ear edge artery of the RT group and the HT group. In order to evaluate respiratory function and acid-base balance, blood gas index including Lac(mmol/L), PH, PO2 (mmHg), PCO2 (mmHg) at different time points (0, 15 min, 6 h and 24 h) after ROSC was analyzed using a blood-gas analyzer.

2.6. Metabolite extraction, derivatization, and analysis for GC–MS

The serum was prepared with the following steps: post-thawing serum sample (100 μL) was mixed with 10 μL L-2-chloro-phenylalanine/methanol (0.3 g/L) as an internal standard and 100 μL methanol/acetonitrile (2:1, v: v). The mixture was thoroughly vortexed for 10 s and sonicated in an ice-water bath for 10 min, followed by centrifugation (12,000 rpm, 4 °C) for 10 min. We added 50 μL of methoxyamine hydrochloride-pyridine (15 g/L) and mixed well. The obtained mixture was placed in a 70 °C water bath for 1 h, then cooled for 15 min. The chemicals derivatized with 50 μL N, *O*-bis(trimethylsilyl)trifluoroacetamide (BSTFA) with 1% trimethylchlorosilane (TMCS) at 70 °C for 1 h and then co-incubated at room temperature for 30 min. The supernatant was collected for GC−MS analysis (7890 A and 5975C, Agilent). To ensure the stability of the system, each analyzed serum sample (5 μL) was mixed as a quality control (QC) sample. QC were injected to condition the platform at the beginning and then monitor the system after almost every six samples. GC-MS/MS parameters were set as following: DB-5MS capillary column (30 m × 250 μm × 0.25 μm, J & Scientific, CA); split ratio (100:1); high purity helium gas with a flow rate of 1.1 ml/min; temperature set at 70 °C for 3 min, then ramped 10 °C/min to 310 °C, and hold for 10min; set inlet temperature at 250 °C; electron impact (EI) ionization voltage at 70eV and ion source temperature at 310 °C; full scan (50–500 *m/z*) [20,21].

2.7. Metabolite extraction and analysis for UPLC-Q-TOF-MS/MS

Serum samples were thawed on the ice. Post-thawing sample (100 μL) was mixed with 10 μL L-2-chloro-phenylalanine/methanol (0.3 g/L) as an internal standard and 100 μL methanol/acetonitrile (2:1, v: v). The mixture was thoroughly vortexed for 10s and sonicated in an ice-water bath for 10 min, followed by centrifugation (12,000 rpm, 4 °C) for 10 min and then added 300 μL methanol/acetonitrile (2:1, v: v) with a vortex for 1 min. After sonication in an ice-water bath for 10 min, serum was allowed to sit at −20 °C for 30 min before being centrifuged (12,000 rpm, 4 °C) for 15 min. Then supernatant was obtained to injection into UPLC-Q-TOF-MS/MS

system (Impact II, Bruker Daltonic Inc.). The QC samples were prepared by adding equivalent portions of the supernatant and then monitor the system after almost every six samples. UPLC-Q-TOF-MS/MS parameters were set as following: Acclaim RSLC 120-C18 chromatographic column (2.2 μm, 120 A, 100 × 2.1 mm, 40 °C, Thermo Scientific); nitrogen as drying gas with a flow rate of 8 L/min; temperature set at 200 °C; electrospray ion source (ESI) voltage at +4900 V in the positive ion mode, −4500 V in the negative ion mode; full scan (20–1000 *m/z*); injection volume (10 μL with flow rate 0.2 ml/min); gradient elution including mobile phase A (0.1% formic acid in water, 2 mmol/L ammonium formate) and mobile phase B (acetonitrile, HPLC grade), the elution scheme as follows: 0–2 min (98% A, 2% B), 2–12 min (98% A to 5% A, 2% B to 50% B), 12–20 min (5% A to 10% A, 50% B to 90% B), 20–30 min (10% A, 90% B), 30–30.1 min (10% A to 98% A, 90% B to 2% B), 30.1–35 min (98% A, 2% B) [22].

2.8. Statisticial data processing, ultivariate pattern recognition and pathway analysis

Metabolomics data obtained from GC-MS/MS and UPLC-Q-TOF-MS/MS were processed by Metaboscape 3.0. The primary parameters were set as follows: retention time as 0–33 min; minimum peak width at 5 s; peak intensity threshold at 1000. Those data were corrected for mass bias by sodium formate and handled according to "80% rule". The final marched peaks were generated exported to an Excel file containing compound name, retention time and corresponding peak intensities. The generated metabolites were tentatively identified based on the public online databases, such as Human Metabolome Database (http://www.hmdb.ca), PubChem database (https://pubchem.ncbi.nlm.nih.gov/) and Kyoto Encyclopedia of Genes and Genomes (KEGG) pathway database (http://www.kegg.jp) by matching mass characteristics and retention time. The drugs, repetitive chemicals and metabolites with more than 30% miss values were removed from analysis. Replacements of missing values were conducted using the missForest R package which is a machine learning-based data imputation algorithm with high efficiency [23]. The total data were normalized by the sum of all peaks and to log10 transformation on MetaboAnalyst 5.0 (http://www.metaboanalyst.ca). The normalized data were used for subsequent statistical analysis.

The processed data were imported into the SIMCA-P version 14.1 (Umetrics, Umeå, Sweden) for principal components analysis (PCA) and orthogonal partial least squares discriminant analysis (OPLS-DA). Furthermore, data was performed for the fold change and heatmap clustering analysis with ggplot2 R package [24] and MetaboAnalyst 5.0. Differential metabolites were screening as follows: VIP value > 1.0, P value < 0.05, FC value > 2 or FC value < 0.66 [25,26]. The metabolic pathways were analyzed using MetaboAnalyst 5.0 based on the differentially expressed metabolites.

3. Results

3.1. Physiologic parameters

Rabbits underwent asphyxial cardiac arrest and resuscitated successfully were randomly assigned to the NT (n = 10) and HT (n = 10) groups. Sham group (n = 6) underwent only general anesthesia and endotracheal intubation. Physiologic parameters were recorded to ensure the consistency under the experimental conditions. As expected, there was no significant difference in baseline body temperature, heart rate, MAP, Lac, PH, PO2 and PCO2 among three groups (Fig. 2). Compared with the NT group, the heart rate being significantly slower during 0.5–6 h post ROSC in the HT group (Fig. 2A), consistent with the decreasing trend of body temperature (Fig. 2B). There was no remarkable difference in MAP levels between NT and HT groups (Fig. 2C). Furthermore, compared with baseline, the Lac level increased notably at 0 h after ROSC (Fig. 2D), while the level of Lac (Fig. 2D) and PO2 (Fig. 2E) decreased significantly at 6 h and 24 h post ROSC in NT and HT groups. In addition, the levels of Lac (Fig. 2D) and PCO2 (Fig. 2F) at 24 h post

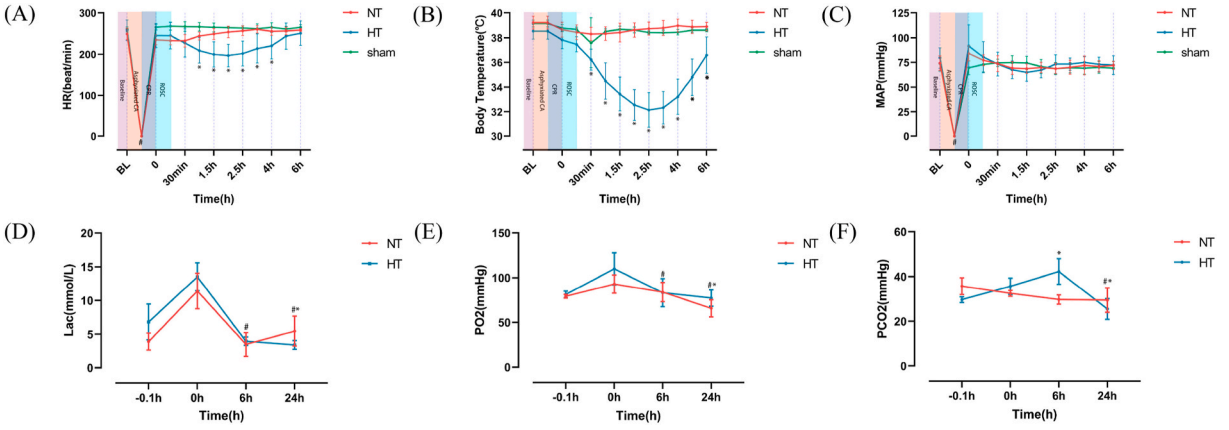

Fig. 2. Physiologic parameters before asphyxial cardiac arrest and after ROSC. (A) HR, (B) Body temperature, (C) MAP, (D) lactic acid, (E) PO2, (F) PCO2. The green, red and blue represent sham, NT and HT group, respectively. #P < 0.05 versus 0 h; *P < 0.05 versus NT group.

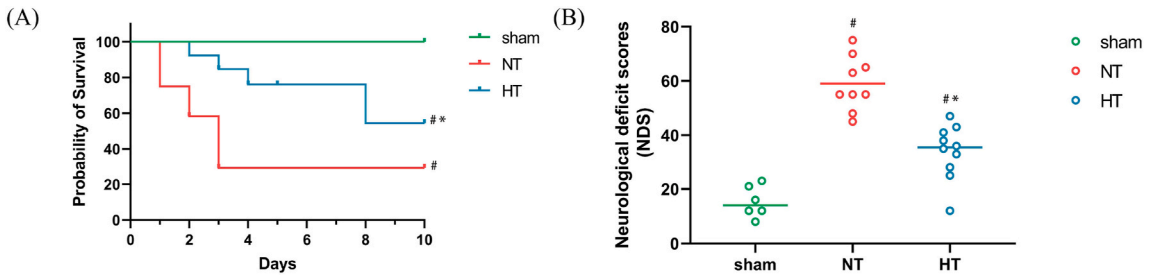

Fig. 3. Survival rate and NDS in different groups. (A) Probability of survival, (B) NDS at 24 h after ROSC. #P < 0.05 versus sham group; *P < 0.05 versus NT group.

ROSC in HT group were lower than those in the NT group, while a significant increase in PO2 level at 24 h post ROSC was seen in the HT group compared with the NT group (Fig. 2E).

Therapeutic hypothermia improves both the survival and neurological outcomes after cardiac arrest. The survival rate of CA rabbits resuscitated successfully in the HT group was significantly higher than that in the NT group (Fig. 3A). The NDS was evaluated at 24 h post ROSC. Compared with the HT group, NDS scores were remarkably increased in the NT group (Fig. 3B).

3.2. *Multivariate data analysis based on UPLC-Q-TOF-MS/MS and GC-MS/MS data in CA rabbits*

An integrated UPLC-Q-TOF-MS/MS and GC-MS/MS based metabolomics approach was adopted to detect the metabolic profiles of serum samples at different time points (15 min, 3 h, 6 h, 24 h) post ROSC within three experimental groups. The principal component analysis (PCA), an unsupervised method of multivariate analysis, was first applied to visualize the metabolic profiles. Remarkable differences of metabolic profiles at 15 min, 3 h, 6 h, 24 h post ROSC were observed among Sham, NT and HT groups from the PCA score plots in both UPLC-Q-TOF-MS/MS (ESI positive modle Fig. 4A–D ESI negative model Fig. 4E–H) and GC-MS/MS (Fig. 4I– L). Tight clustering of QC samples indicated that the quality of metabolomic data is reproducible and stability.

Multivariate statistical analysis by orthogonal partial least squares discriminant analysis (OPLS-DA) supervised pattern recognition method was introduced to maximize the separation and identify the difference of serum metabolic profiles in three groups. As shown in Fig. 5, the score plot revealed that the serum metabolic profiles at 15 min, 3 h, 6 h and 24 h post ROSC in three groups were significantly different in both UPLC-Q-TOF-MS/MS (ESI positive model Fig. 5A–D, ESI negative model Fig. 5I– L) and GC-MS/MS

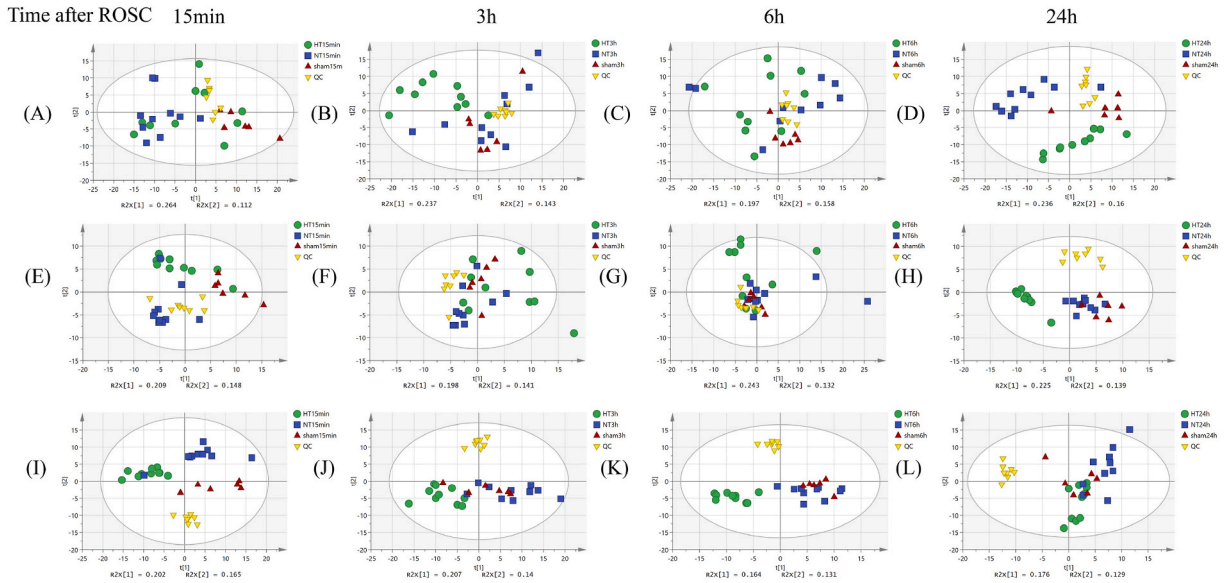

Fig. 4. PCA analysis of UPLC-Q-TOF-MS/MS and GC-MS/MS data from serum samples at 15 min, 3 h, 6 h and 24 h post ROSC of asphyxial CA within three experimental groups. (A–D) PCA score plot of UPLC-Q-TOF-MS/MS (ESI+) mode data, (*M*–P) PCA analysis derived form UPLC-Q-TOF-MS/MS (ESI-) mode data, (I–L) PCA score plot using GC-MS/MS data.

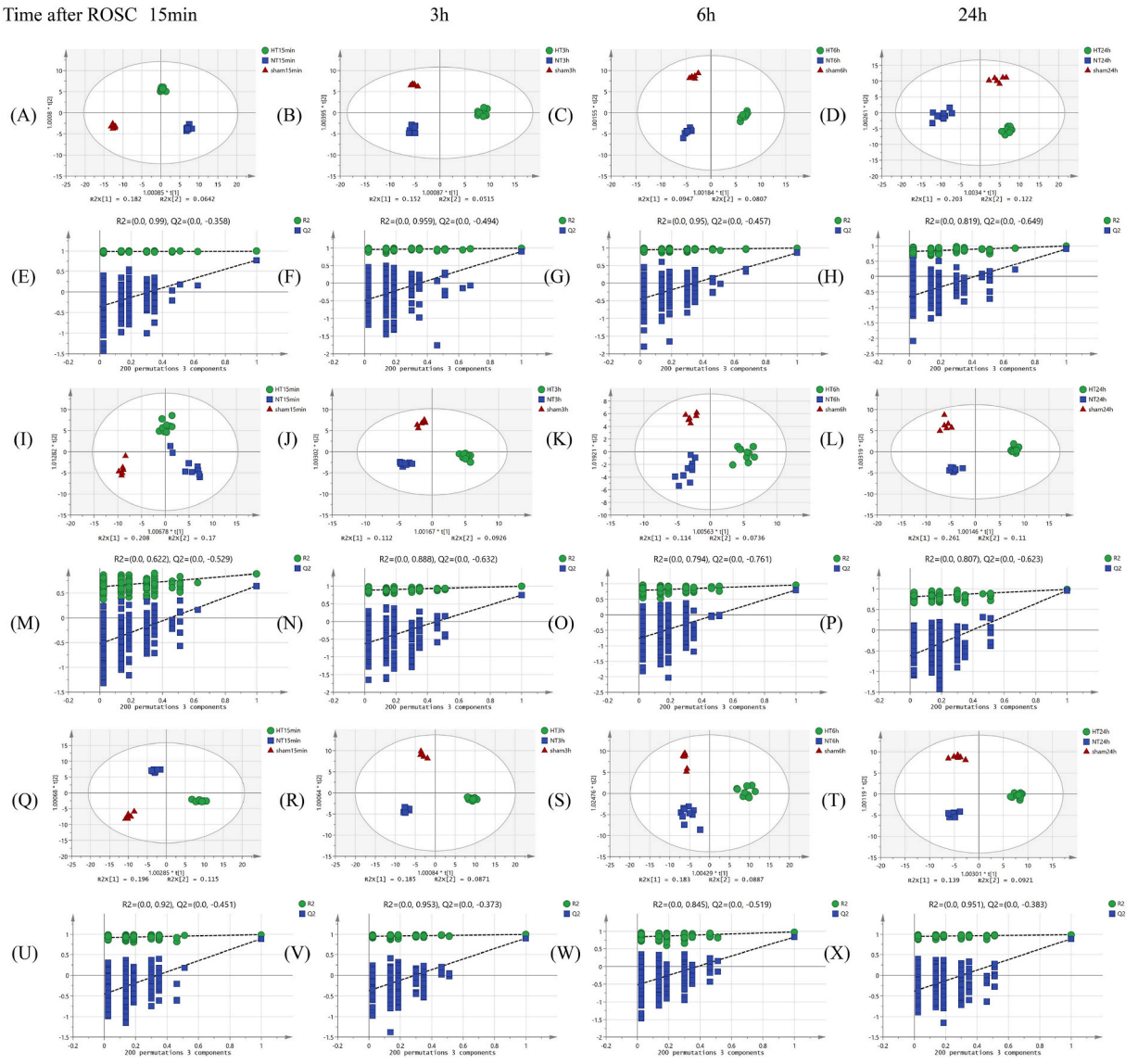

Fig. 5. OPLS-DA of asphyxial CA serum based on UPLC-Q-TOF-MS/MS and GC-MS/MS data at different time points (15 min, 3 h, 6 h, 24 h post ROSC) within three experimental groups. (A–D) OPLS-DA score plot of UPLC-Q-TOF-MS/MS (ESI+) data, (*E*–H) the 200-permutation test of UPLC-Q-TOF-MS/MS (ESI+) data, (I–L) OPLS-DA score plot of UPLC-Q-TOF-MS/MS (ESI-) data, (*M*–P) the 200-permutation test of UPLC-Q-TOF-MS/MS (ESI+) data, (Q–T) OPLS-DA score plot of GC-MS/MS data, (U–X) the 200-permutation test of GC-MS/MS.

(Fig. 5Q– T). High statistical values of the R2Y and Q2 (Q2 > 0.5 and the differences between R2Y and Q2 <0.3) in the OPLS-DA models manifested the goodness and the predictive ability respectively [15 min, UPLC-Q-TOF-MS/MS ESI+, R2Y = 0.997, Q2 = 0.816, UPLC-Q-TOF-MS/MS ESI-, R2Y = 0.932, Q2 = 0.716, GC-MS/MS, R2Y = 0.995, Q2 = 0.874; 3 h, UPLC-Q-TOF-MS/MS ESI+, R2Y = 0.994, Q2 = 0.789, UPLC-Q-TOF-MS/MS ESI-, R2Y = 0.989, Q2 = 0.723, GC-MS/MS, R2Y = 0.997, Q2 = 0.839; 6 h, UPLC-Q-TOF-MS/MS ESI+, R2Y = 0.997, Q2 = 0.874, UPLC-Q-TOF-MS/MS ESI-, R2Y = 0.957, Q2 = 0.614, GC-MS/MS, R2Y = 0.96, Q2 = 0.772; 24 h, UPLC-Q-TOF-MS/MS ESI+, R2Y = 0.982, Q2 = 0.843, UPLC-Q-TOF-MS/MS ESI-, R2Y = 0.992, Q2 = 0.881, GC-MS/MS, R2Y = 0.994, Q2 = 0.843]. Furthermore, the permutation test (200 times) was performed to validate the generated models. For the permuted R2 and Q2, all the values were lower than their corresponding original ones, the intercepted value of Q2 on the vertical axis was below 0, indicating that the supervised OPLS-DA models were not overfitted (Fig. 5E–H, 5M − 5 P and 5U-5X).

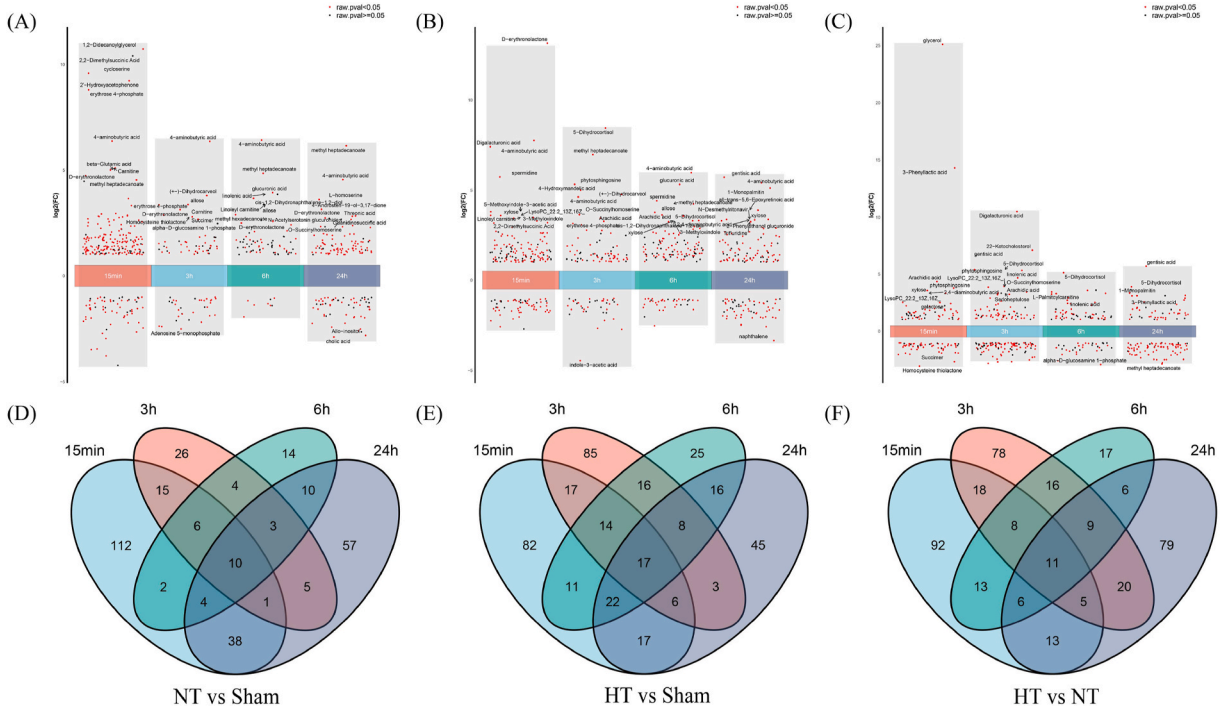

Fig. 6. Volcano plot of three groups at different time points. (A) NT versus sham; (B) HT versus sham; (C) HT versus NT (Red presents $P < 0.05$; black represents $P \geq 0.05$). Wenn diagram in the comparison of three groups. (D) NT versus sham; (E) HT versus sham; (F) HT versus NT.

To compare and identify the metabolites in the sham, NT and HT groups, OPLS-DA and a 200-times permutation test were used in the NT versus sham, HT versus sham and HT versus NT groups. The results indicated that these models could identify the potential metabolites in the various comparison groups and time points (supplementary Fig. 1-6). According to the corresponding variable importance of projection (VIP) value greater than 1.0 (VIP>1), potential differential metabolites were selected.

3.3. Analysis of serum differential metabolites between every two groups (NT vs sham, HT vs sham and HT vs NT) at 15 min, 3 h, 6 h, 24 h post ROSC

Based on screening criteria of fold change≥1.5 or fold change<0.66, VIP>1 and p value < 0.05, the differential metabolites detected by UPLC-Q-TOF-MS/MS and GC-MS/MS were screened for further study between every two groups (NT vs sham, HT vs sham and HT vs NT) at 15 min, 3 h, 6 h and 24 h post ROSC. As a result, compared with the sham group, a total of 188, 70, 53 and 128 differential expression endogenous metabolites were identified in the NT group at 15 min, 3 h, 6 h and 24 h post ROSC respectively (Fig. 6A, Supplementary Table 1), 186, 166, 129 and 134 differential metabolites were screened in the HT group at various time points (15 min, 3 h, 6 h and 24 h) after ROSC respectively (Fig. 6B, Supplementary Table 2). Compared with the NT group, a total of 166, 165, 86 and 149 differential metabolites were detected in the HT group at 15 min, 3 h, 6 h and 24 h post ROSC respectively (Fig. 6C, Supplementary Table 3). The Venn diagrams of differentially expressed metabolites at 15 min, 3 h, 6 h and 24 h post ROSC shown the number of overlapping metabolites between the NT and sham group (Fig. 6D), the HT and sham group (Fig. 6E), the HT and NT group (Fig. 6F). The common differential metabolites at 15 min, 3 h, 6 h and 24 h post ROSC were shown in Table 1.

In order to visualize the clustering in serum metabolites in the sham, NT and HT groups, the hierarchical clustering analysis of differential metabolites with a VIP score >1 was used to further depict the clustering effect between groups at 15 min (Fig. 7A), 3 h (Fig. 7B) 6 h (Figs. 7C) and 24 h (Fig. 7D) post ROSC, showed the clear separation for each alignment. Interestingly, the relative intensive of differential metabolites showed well clustering, which indicated the reliability of the OPLS-DA model for distinguishing different metabolic phenotypes in sham, NT and HT groups at 15 min, 3 h, 6 h and 24 h post ROSC.

Table 1
Differential metabolites detected by UPLC-Q-TOF-MS/MS and GC-MS/MS at different time points after ROSC.

compound name	Formula	MW (g/mol)	RT (min)	15min			3 h			6 h			24 h		
				FC	*P*	VIP	FC	*P*	VIP	FC	P	VIP	FC	*P*	VIP
NT vs sham															
4-aminobutyric acid	C4H9NO2	103.1	16.06	83.051	8.29E-08	1.51323	82.409	4.85E-06	1.54548	85.96	2.70E-07	1.72634	23.566	1.69E-08	1.95666
Carnitine	C7H15NO3	161.2	12.53	34.401	7.84E-05	1.46736	7.4301	7.53E-12	2.09138	5.1388	8.46E-06	2.21434	5.4905	8.43E-06	2.08912
D-erythronolactone	C4H6O4	118.1	6.69	26.819	1.28E-03	1.31714	8.8442	3.88E-02	1.21092	5.7394	4.64E-02	1.21035	7.1179	4.76E-03	1.47951
glucose-6-phosphate	C6H13O9P	260.1	26.24	5.1823	1.11E-03	1.19961	2.4208	3.66E-05	1.83807	2.1679	3.42E-02	1.23801	2.775	2.27E-04	1.65567
indole-3-acetic acid	C10H9NO2	175.2	15.96	0.21433	5.13E-06	1.81342	0.19233	1.38E-04	1.60221	0.26141	7.02E-05	1.91925	0.16445	9.26E-15	2.37611
Isoleucine	C6H13NO2	131.2	8.08	0.65766	4.71E-02	1.33319	0.54864	3.56E-05	1.9846	0.4022	1.66E-04	2.13706	0.60173	1.58E-03	1.8098
methyl heptadecanoate	C18H36O2	284.5	17.74	23.381	4.21E-09	1.78647	5.5078	1.61E-02	1.24054	29.088	1.40E-03	1.78846	71.007	2.69E-04	1.79885
N-Acetyl-beta-D-mannosamine	C8H15NO6	221.2	25.59	6.2983	8.34E-05	1.33072	3.0464	2.27E-03	1.54532	2.6263	1.98E-03	1.39258	2.7296	1.30E-04	1.71281
O-phosphonothreonine	C4H10NO6P	199.1	11.26	4.4261	3.23E-04	1.63147	3.6064	8.39E-04	1.38781	3.6833	1.55E-03	1.67139	3.1482	7.30E-03	1.31798
sorbose	C6H12O6	180.2	30.1	5.5559	5.46E-08	1.68279	2.7174	1.84E-06	1.8676	2.5992	2.83E-05	2.09738	3.9907	7.60E-06	2.03188
HT vs sham															
2,4-diaminobutyric acid	C4H10N2O2	118.1	19.2	6.2586	2.04E-05	1.44928	9.5675	4.35E-11	1.89838	9.2968	5.14E-09	1.65395	10.267	1.70E-05	1.76189
2-aminoethanethiol	C2H7NS	77.2	5.95	0.57598	9.16E-04	1.35948	0.57131	4.23E-04	1.65929	0.61312	2.54E-05	1.8093	0.53409	7.41E-07	2.03414
2-hydroxybutanoic acid	C4H8O3	104.1	6.63	0.64454	3.11E-05	1.50867	0.57845	1.46E-04	1.70168	0.52737	1.60E-06	1.91887	0.61604	3.85E-06	2.0011
3-Aminoisobutyric acid	C4H9NO2	103.1	5.81	0.46199	8.48E-04	1.3477	0.52593	2.03E-03	1.50746	0.47976	4.79E-04	1.73381	0.57678	4.49E-03	1.56933
4-aminobutyric acid	C4H9NO2	103.1	16.06	170	9.03E-07	1.30216	24.783	5.65E-08	1.58772	63.09	1.15E-05	1.15948	42.726	4.79E-08	1.76417
4-Hydroxybenzoic acid	C7H6O3	138.1	13.16	0.38899	1.59E-02	1.28199	0.40246	1.48E-02	1.32857	0.44935	1.87E-02	1.49915	0.30087	6.85E-03	1.85633
Carnitine	C7H15NO3	161.2	12.53	5.5864	1.25E-05	1.54728	6.8644	9.27E-13	1.99691	6.2616	1.66E-05	1.74218	6.0033	1.03E-05	1.90869
Glucoheptonic acid	C7H14O8	226.2	29.4	6.6432	8.94E-04	1.17401	3.9289	1.30E-05	1.70524	2.6327	2.21E-02	1.02427	2.9519	1.07E-03	1.70364
glycerol	C3H8O3	92.1	7.75	6.1786	6.09E-04	1.32716	6.9415	3.11E-13	1.99058	6.4046	1.20E-12	2.0051	6.5272	8.08E-14	2.13168
indole-3-acetic acid	C10H9NO2	175.2	15.96	0.13588	1.35E-13	1.72677	0.045696	8.74E-10	1.87025	0.12136	6.08E-08	1.99871	0.16415	4.60E-14	2.17145
Isoleucine	C6H13NO2	131.2	8.08	0.51388	1.91E-03	1.28932	0.5506	2.71E-05	1.72368	0.52266	6.53E-05	1.67901	0.47747	1.18E-05	1.9179
O-phosphonothreonine	C4H10NO6P	199.1	11.26	2.931	4.11E-03	1.11992	2.6885	1.70E-03	1.36997	2.4762	2.14E-02	1.07908	6.4596	2.70E-04	1.63142

(*continued on next page*)

Table 1 (*continued*)

compound name	Formula	MW (g/mol)	RT (min)	15min			3 h			6 h			24 h		
				FC	*P*	VIP	FC	*P*	VIP	FC	P	VIP	FC	*P*	VIP
phosphate	O4P-3	94.971	7.77	0.31148	8.84E-04	1.38698	0.15728	1.61E-16	2.04122	0.17358	5.40E-17	2.07401	0.26604	1.97E-05	1.87951
Phenylpyruvic acid	C9H8O3	164.2	2.12	3.34	7.32E-04	1.57426	3.1633	1.16E-02	1.23332	2.9733	1.95E-04	1.74605	6.1255	3.41E-07	2.00923
Trifluridine	C10H11F3N2O5	296.2	11.61	3.336	1.50E-03	1.34313	2.0425	3.76E-03	1.71513	8.4397	1.22E-06	1.89901	9.6103	1.65E-07	1.68125
di-Hydroxymelatonin	C13H16N2O4	264.3	13.04	0.41843	7.60E-06	1.87104	0.21274	1.62E-05	2.29319	0.31619	1.08E-04	2.01748	0.58654	4.49E-04	1.62735
3′,4′-Dihydrodiol	C15H14N2O4	286.3	15.56	0.531	7.29E-03	1.5604	2.7288	3.87E-02	1.52994	3.825	2.82E-04	1.65737	4.5313	8.33E-06	1.4083
HT vs NT															
2,4-diaminobutyric acid	C4H10N2O2	118.1	19.2	10.095	1.68E-06	1.69854	8.8109	1.25E-08	1.82223	9.5485	1.32E-09	1.74045	3.767	7.53E-04	1.70913
22-Ketocholesterol	C27H44O2	400.6	5.34	4.4484	1.83E-05	1.68209	136.1	6.81E-04	1.30392	3.9373	3.27E-05	1.68905	3.1848	2.95E-02	1.1516
alpha-D-glucosamine1-phosphate	C6H14NO8P	259.1	24.34	0.20256	8.73E-04	1.44182	0.17689	8.87E-03	1.04647	0.1345	2.28E-05	1.60442	0.16009	9.19E-03	1.24566
Arachidic acid	C20H40O2	312.5	26.55	20.398	2.52E-05	1.448	10.895	7.67E-12	1.71578	12.004	2.23E-11	1.78969	8.8236	1.24E-03	1.01887
beta-Mannosylglycerate	C9H16O9	268.2	18.04	4.5761	1.11E-03	1.64433	4.436	3.18E-04	1.30233	3.0893	1.37E-04	1.42125	2.2755	1.37E-04	1.65663
glycerol	C3H8O3	92.1	7.75	35,800,000	1.39E-05	1.6682	6.8938	9.58E-18	1.96918	6.4432	4.87E-17	2.09345	6.384	1.93E-18	2.29768
L-4-Hydroxyphenylglycine	C8H9NO3	167.2	8.11	0.57457	1.34E-03	1.30133	0.49759	6.59E-05	1.49224	0.64628	6.86E-04	1.47949	0.60785	7.75E-04	1.56517
phosphate	O4P-3	95	7.77	0.33523	5.39E-05	1.60228	0.1449	1.54E-17	1.92267	0.16961	2.61E-22	2.1463	0.24515	4.30E-08	2.11966
Sedoheptulose	C7H14O7	210.2	21.87	4.7195	6.99E-04	1.35944	10.122	3.83E-07	1.48583	5.7778	3.51E-05	1.41622	3.6159	1.94E-05	1.85571
Capric acid	C10H20O2	172.3	11.69	0.55482	7.77E-03	1.26652	0.23044	9.82E-04	1.44931	0.25164	1.45E-02	1.9845	0.32639	2.61E-04	1.64697
Trifluridine	C10H11F3N2O5	296.2	11.61	2.0909	1.51E-02	1.44365	2.3566	2.93E-03	1.81223	5.3419	1.70E-05	2.24037	5.1576	1.17E-06	1.61389

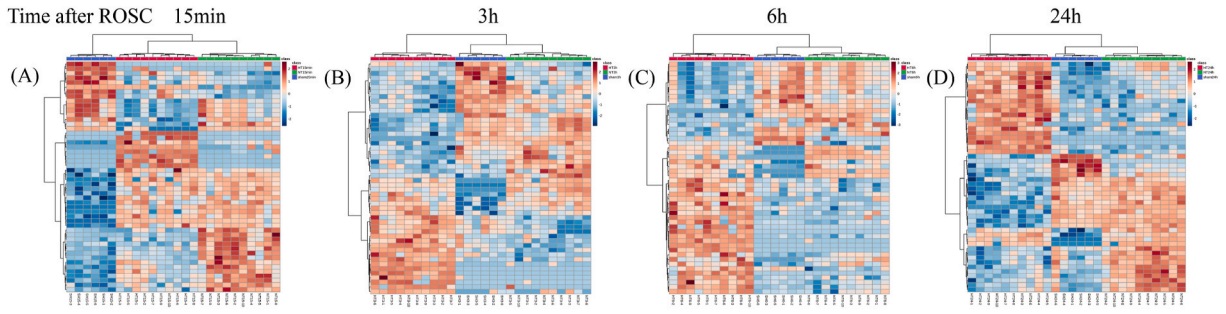

Fig. 7. The hierarchical clustering analysis on differential expression of metabolites in each group at 15 min (A), 3 h (B), 6 h (C) and 24 h (D) post ROSC. Cluster analysis using euclidean distance and Ward algorithm are showed as: each column represents a rabbit, and each row represents an individual metabolite. The relative metabolite level is depicted according to the color scale. Red and blue indicate up-regulation and down-regulation, respectively.

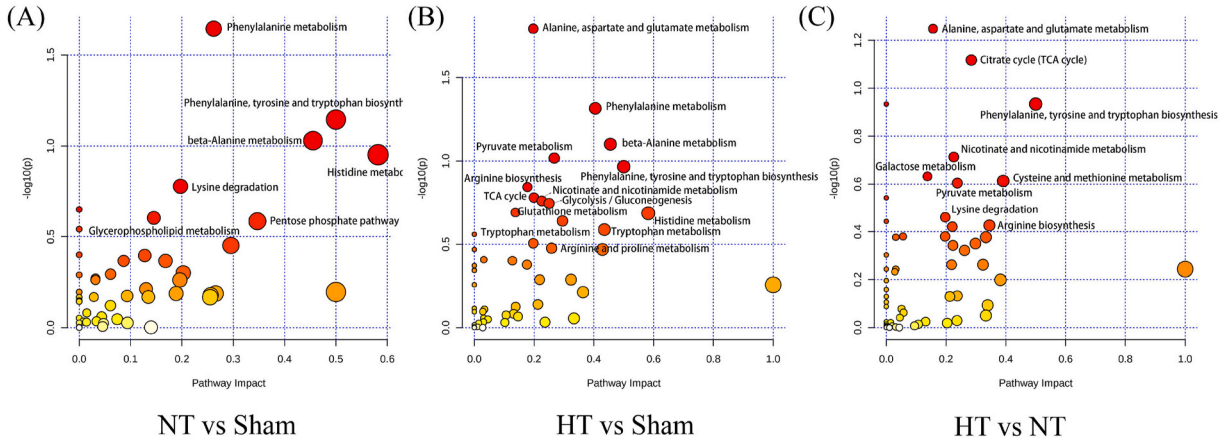

Fig. 8. The KEGG pathway analysis between every two groups. (A) NT versus sham; (B) HT versus sham; (C) NT versus HT.

3.4. Altered metabolic pathway related to CA

To explore the potential metabolic pathways involved in CA, metabolic pathways were further analyzed in MetaboAnalyst 5.0 for KEGG pathway analysis and network topology analysis. According to impact >0.1, phenylalanine, tyrosine and tryptophan biosynthesis, pyrimidine metabolism, ascorbate and aldarate metabolism and phenylalanine metabolism metabolic pathways were screened out in NT group compared with sham group at 15 min, 3 h, 6 h and 24 h post ROSC respectively (Supplementary Fig. 7A-7D). Compared with the NT group, TCA, phenylalanine, tyrosine and tryptophan biosynthesis, alanine, aspartate and glutamate metabolism and nicotinate and nicotinamide metabolism pathways were detected in the HT group at 15 min, 3 h, 6 h and 24 h post ROSC respectively (Supplementary Fig. 7I-7L). There was pyruvate metabolism, tryptophan metabolism, phenylalanine metabolism and beta-Alanine metabolism metabolic pathways in the HT group at 15 min, 3 h, 6 h and 24 h post ROSC respectively (Supplementary Fig. 7E-7H). Combining to all the time factors, metabolite pathway analysis showed that phenylalanine metabolism, alanine, aspartate and glutamate metabolism and TCA pathways were enriched in NT vs sham (Fig. 8A), HT vs sham (Fig. 8B) and HT vs NT (Fig. 8C) respectively. There are 16 common metabolic pathways, which are phenylalanine metabolism, phenylalanine, tyrosine and tryptophan biosynthesis, histidine metabolism, lysine degradation, pentose phosphate pathway (PPP), cysteine and methionine metabolism, galactose metabolism, TCA, pyrimidine metabolism, tryptophan metabolism glycolysis/gluconeogenesis, starch and sucrose metabolism, pentose and glucuronate interconversions, glutathione metabolism, vitamin B6 metabolism and tyrosine metabolism. To clearly elucidate the possible underlying mechanism, the schematic overview of differential metabolites and major metabolic pathway related with the NT group (Fig. 9A) and the HT group (Fig. 9B) was reconstructed.

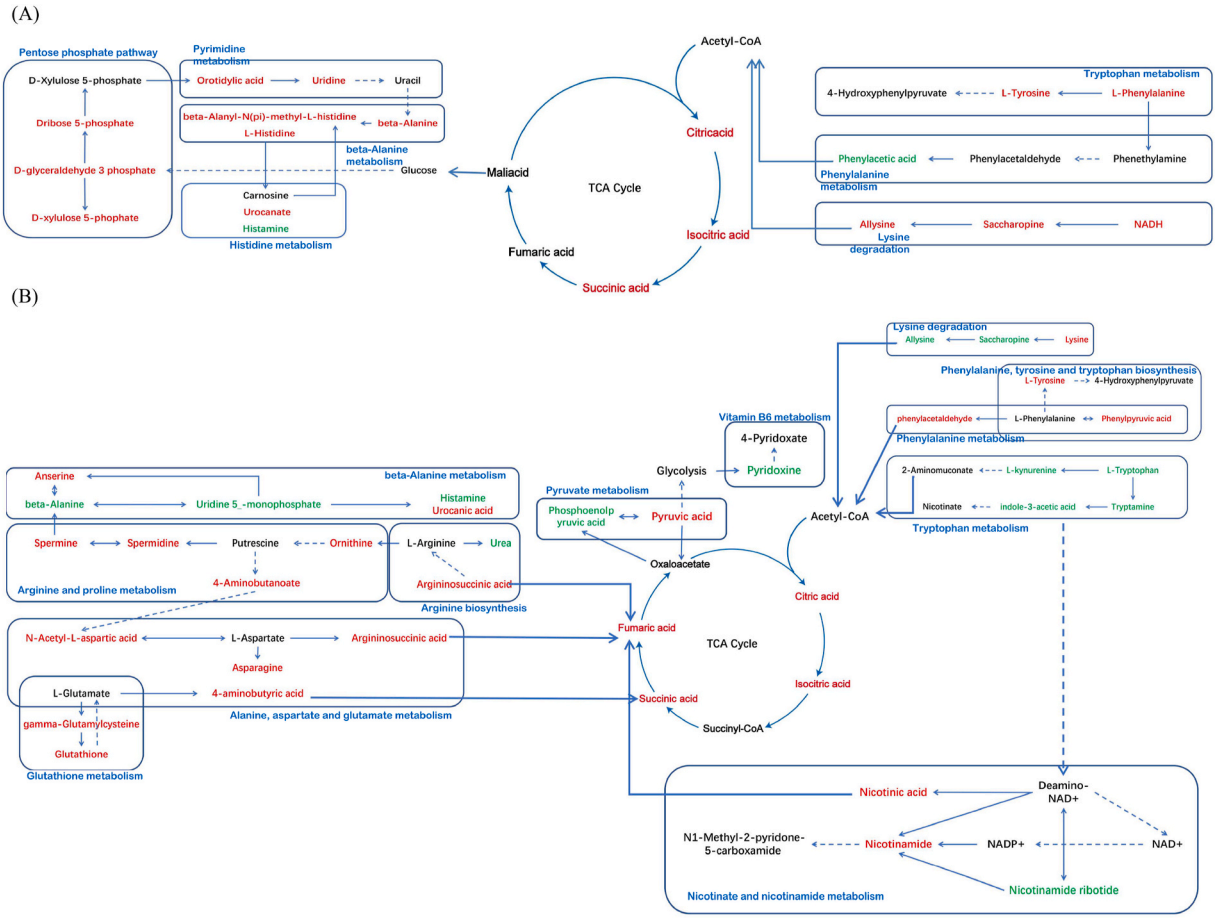

Fig. 9. Schematic representation of the metabolites and major metabolic pathways changes. (A) NT vs sham; (B) HT vs sham. Red presents increased metabolite; green represents decreased metabolite; black represents no detected metabolite.

4. Discussion

CA is a relatively common adverse event in intensive care medicine. The prevalence of sudden cardiac death in China is up to 40.7/100,000 annually [27]. Among the initial treatment of the CA, cardiopulmonary resuscitation (CPR) plays an important role. However, several pathological features including myocardial dysfunction, ischemia/reperfusion injury, permanent brain injury and persistent precipitating pathophysiology occurred during CA and CPR [28–30]. Many patients died from multiple organ failures due to metabolic disorders, oxidative stress and inflammatory responses [31–33]. Target temperature management has been the cornerstone of neuroprotection in patients after ROSC for the past years [34,35], but the exact mechanism remains unknown.

Our study demonstrated that the PPP, phenylalanine metabolism, phenylalanine, tyrosine and tryptophan biosynthesis, beta-alanine metabolism, histidine metabolism are differentially expressed in the NT group. The PPP is responsible for the ribose synthesis. Glucose 6-phosphate dehydrogenase (G-6-PD) is the main enzymes in the oxidative PPP [36]. Previous study showed that G-6-PD and ribose can improve the cardiac function and reduce reactive oxygen species (ROS) [37]. At this study, our finding represented that PPP varies more significantly at 15 min. It indicates that serious oxidative stress occurs during the ROSC. Moreover, β-alanine, as a neurotransmitter, can suppress the uptake of taurine and decrease the regulatory effect on Ca^{2+}, whose excessive accumulation can enhance the myocardial cytotoxicity [38,39]. Histidine, one of the downstream metabolites, contributes to vascular dilatation and blood pressure reduction, thus reducing the burden on the heart [40,41]. Our findings highlighted an obvious up-regulation of β-alanine metabolism at 24 h after ROSC and down-regulation of histidine metabolism at 15 min, 3 h and 24 h after ROSC in the NT group compared with the sham group. This suggested that elevated β-alanine and reduced histidine levels may contribute to further cardiomyocyte injury. In addition, L-phenylalanine is oxidized to another essential amino acid, L-tyrosine [42]. However, free L-tyrosine results in production of nitro tyrosine, which can lead to the neurotoxicity frequently found in neurological clinical studies [43]. Our results found that phenylalanine, tyrosine and tryptophan biosynthesis and phenylalanine metabolism regulate the increase of L-tyrosine, which may explain the poor prognosis of cardiac arrest.

Unlike the NT group, critical KEGG pathways in the HT group displayed differently. Although the virtually same changes of the phenylalanine metabolism, beta-alanine metabolism, phenylalanine, tyrosine and tryptophan biosynthesis was confirmed that ROSC

leads to the cardiac damage and nerve injury. There were other pathways enriched, including alanine, aspartate and glutamate metabolism, pyruvate metabolism, arginine biosynthesis, TCA cycle, nicotinate and nicotinamide metabolism, glycolysis/gluconeogenesis, glutathione metabolism, tryptophan metabolism. The human brain is an extremely complex organ that highly dependent on the energy from pyruvate and glutamate metabolism [44,45]. Compared with the NT group, changes of alanine, aspartate and glutamate metabolism, as well as pyruvate metabolism were observed to generate ATP in the HT group. While, PPP can provide ATP with relatively low efficiency in the NT group, making it difficult to reach the demands of the brain repair and heart restore [46,47]. Intriguingly, we found that catabolism of tryptophan occurs at 3 h, 6 h and 24 h in the HT group. Studies have confirmed that metabolism of tryptophan plays an important negative feedback regulatory role in the central nervous system (CNS), inhibiting the neuroinflammation [48,49]. Additionally, our results showed that nicotinamide and nicotinic acid increased at 3 h. Previous studies indicated that these substances can improve cardiac function and limit neuron damage caused by oxidative stress [50–52]. Importantly, despite the no significant changes in L-arginine, we found increased up-stream argininosuccinic acid content and decreased down-stream urea consumption. L-arginine is the natural substrate for generating nitric oxide (NO), which is a key regulator of ischemia/reperfusion injury recovery and neuroprotection [53–55]. Thus, we deduce that mild therapeutic hypothermia improved the survival and neurological outcomes following cardiac arrest through regulating alanine, aspartate and glutamate metabolism, pyruvate metabolism, arginine biosynthesis, tryptophan metabolism and nicotinate and nicotinamide metabolism.

5. Conclusion

In the present study, we demonstrated that the mild therapeutic hypothermia improved the survival and neurological outcomes in rabbits with cardiac arrest. Metabolomics analysis revealed significant differences in the metabolic profiles among sham, NT and HT groups. alanine, aspartate and glutamate metabolism, pyruvate metabolism, arginine biosynthesis, tryptophan metabolism and nicotinate and nicotinamide metabolism were involved in the protective effects of mild therapeutic hypothermia on neurologic injury induced by cardiac arrest. Collectively, our study offers new insights into the mechanism of therapeutic hypothermia for cardiac arrest from the perspective of metabolomics.

Author contribution statement

Yiyuan Zhang: Analyzed and interpreted the data, Wrote the paper, Drafting the article. **Yang Feng**: Performed the experiments, Wrote the Paper. **Fang Chen, Jiang Yu, Xiehong Liu** and **Yanjuan Liu**: Contributed reagents, materials, analysis tools or data. **Jielin Ouyang**: Analyzed and interpreted the data. **Mingyu Liang**: Performed the experiments. **Yiming Zhu**: Conceived and designed the experiments. **Lianhong Zou**: Conceived and designed the experiments, Critically revising its important intellectual content, Final approval of the version submitted.

Funding statement

This work was financially supported by Natural Science Foundation of Hunan Province (2022JJ30346), the Key Project of Hunan Provincial Science and Technology Innovation (No. 2020SK1010). Scientific Research Program of Health Commission of Hunan Province (No. B 202310007618).

Data availability statement

Data will be made available on request.

Declaration of competing interest

The authors declare that they have no known competing financial interests or personal relationships that could have appeared to influence the work reported in this paper

Appendix A. Supplementary data

Supplementary data to this article can be found online at https://doi.org/10.1016/j.heliyon.2023.e16247.

References

[1] P.B. Forgacs, H.P. Frey, A. Velazquez, S. Thompson, D. Brodie, V. Moitra, L. Rabani, S. Park, S. Agarwal, M.C. Falo, N.D. Schiff, J. Claassen, Dynamic regimes of neocortical activity linked to corticothalamic integrity correlate with outcomes in acute anoxic brain injury after cardiac arrest, Ann Clin Transl Neurol 4 (2) (2017) 119–129, https://doi.org/10.1002/acn3.385.

[2] M. Stasiowski, Ł. Głowacki, J. Gąsiorek, D. Majer, E. Niewiadomska, S. Król, J. Żak, A. Missir, L.K. Prof, P.J. Prof, B.O. Grabarek, General health condition of patients hospitalized after an incident of in-hospital or out-of hospital sudden cardiac arrest with return of spontaneous circulation, Clin. Cardiol. 44 (9) (2021) 1256–1262, https://doi.org/10.1002/clc.23680.

[3] M. Zhou, P. Wang, Z. Yang, H. Wu, Z. Huan, Spontaneous hypothermia ameliorated inflammation and neurologic deficit in rat cardiac arrest models following resuscitation, Mol. Med. Rep. 17 (2) (2018) 2127–2136, https://doi.org/10.3892/mmr.2017.8113.

[4] N.T. Lee, C. Selan, J.S.J. Chia, S.A. Sturgeon, D.K. Wright, A. Zamani, M. Pereira, H.H. Nandurkar, M. Sashindranath, Characterization of a novel model of global forebrain ischaemia-reperfusion injury in mice and comparison with focal ischaemic and haemorrhagic stroke, Sci. Rep. 10 (1) (2020), 18170, https://doi.org/10.1038/s41598-020-75034-4.

[5] N. Mongardon, V. Lemiale, D. Borderie, A. Burke-Gaffney, S. Perbet, N. Marin, J. Charpentier, F. Pène, J.D. Chiche, J.P. Mira, A. Cariou, Plasma thioredoxin levels during post-cardiac arrest syndrome: relationship with severity and outcome, Crit. Care 17 (1) (2013) R18, https://doi.org/10.1186/cc12492.

[6] J. Arrich, H. Herkner, D. Müllner, W. Behringer, Targeted temperature management after cardiac arrest. A systematic review and meta-analysis of animal studies, Resuscitation 162 (2021) 47–55, https://doi.org/10.1016/j.resuscitation.2021.02.002.

[7] K.H. Polderman, J. Varon, Confusion around therapeutic temperature management hypothermia after in-hospital cardiac arrest? Circulation 137 (3) (2018) 219–221, https://doi.org/10.1161/circulationaha.117.029656.

[8] M.S. Sekhon, P.N. Ainslie, D.E. Griesdale, Clinical pathophysiology of hypoxic ischemic brain injury after cardiac arrest: a "two-hit" model, Crit. Care 21 (1) (2017) 90, https://doi.org/10.1186/s13054-017-1670-9.

[9] M.G. Silverman, B.M. Scirica, Cardiac arrest and therapeutic hypothermia, Trends Cardiovasc. Med. 26 (4) (2016) 337–344, https://doi.org/10.1016/j.tcm.2015.10.002.

[10] M.M. Rinschen, J. Ivanisevic, M. Giera, G. Siuzdak, Identification of bioactive metabolites using activity metabolomics, Nat. Rev. Mol. Cell Biol. 20 (6) (2019) 353–367, https://doi.org/10.1038/s41580-019-0108-4.

[11] W.B. Dunn, D.I. Broadhurst, H.J. Atherton, R. Goodacre, J.L. Griffin, Systems level studies of mammalian metabolomes: the roles of mass spectrometry and nuclear magnetic resonance spectroscopy, Chem. Soc. Rev. 40 (1) (2011) 387–426, https://doi.org/10.1039/b906712b.

[12] W.B. Dunn, D. Broadhurst, P. Begley, E. Zelena, S. Francis-McIntyre, N. Anderson, M. Brown, J.D. Knowles, A. Halsall, J.N. Haselden, A.W. Nicholls, I.D. Wilson, D.B. Kell, R. Goodacre, Procedures for large-scale metabolic profiling of serum and plasma using gas chromatography and liquid chromatography coupled to mass spectrometry, Nat. Protoc. 6 (7) (2011) 1060–1083, https://doi.org/10.1038/nprot.2011.335.

[13] E.C. Chan, K.K. Pasikanti, J.K. Nicholson, Global urinary metabolic profiling procedures using gas chromatography-mass spectrometry, Nat. Protoc. 6 (10) (2011) 1483–1499, https://doi.org/10.1038/nprot.2011.375.

[14] I. Laíns, M. Gantner, S. Murinello, J.A. Lasky-Su, J.W. Miller, M. Friedlander, D. Husain, Metabolomics in the study of retinal health and disease, Prog. Retin. Eye Res. 69 (2019) 57–79, https://doi.org/10.1016/j.preteyeres.2018.11.002.

[15] M. Chenoune, F. Lidouren, C. Adam, S. Pons, L. Darbera, P. Bruneval, B. Ghaleb, R. Zini, J.L. Dubois-Randé, P. Carli, B. Vivien, J.D. Ricard, A. Berdeaux, R. Tissier, Ultrafast and whole-body cooling with total liquid ventilation induces favorable neurological and cardiac outcomes after cardiac arrest in rabbits, Circulation 124 (8) (2011) 901–911, https://doi.org/10.1161/circulationaha.111.039388.

[16] C.H. Huang, M.S. Tsai, C.Y. Chiang, Y.J. Su, T.D. Wang, W.T. Chang, H.W. Chen, W.J. Chen, Activation of mitochondrial STAT-3 and reduced mitochondria damage during hypothermia treatment for post-cardiac arrest myocardial dysfunction, Basic Res. Cardiol. 110 (6) (2015) 59, https://doi.org/10.1007/s00395-015-0516-3.

[17] K. Hayashida, M. Sano, N. Kamimura, T. Yokota, M. Suzuki, S. Ohta, K. Fukuda, S. Hori, Hydrogen inhalation during normoxic resuscitation improves neurological outcome in a rat model of cardiac arrest independently of targeted temperature management, Circulation 130 (24) (2014) 2173–2180, https://doi.org/10.1161/circulationaha.114.011848.

[18] A.J. Baker, M.H. Zornow, M.R. Grafe, M.S. Scheller, S.R. Skilling, D.H. Smullin, A.A. Larson, Hypothermia prevents ischemia-induced increases in hippocampal glycine concentrations in rabbits, Stroke 22 (5) (1991) 666–673, https://doi.org/10.1161/01.str.22.5.666.

[19] X. Wei, L. Duan, L. Bai, M. Tian, W. Li, B. Zhang, Effects of exogenous hydrogen sulfide on brain metabolism and early neurological function in rabbits after cardiac arrest, Intensive Care Med. 38 (11) (2012) 1877–1885, https://doi.org/10.1007/s00134-012-2714-x.

[20] F. Segovia-Miranda, H. Morales-Navarrete, M. Kücken, V. Moser, S. Seifert, U. Repnik, F. Rost, M. Brosch, A. Hendricks, S. Hinz, C. Röcken, D. Lütjohann, Y. Kalaidzidis, C. Schafmayer, L. Brusch, J. Hampe, M. Zerial, Three-dimensional spatially resolved geometrical and functional models of human liver tissue reveal new aspects of NAFLD progression, Nat. Med. 25 (12) (2019) 1885–1893, https://doi.org/10.1038/s41591-019-0660-7.

[21] J. Ye, J. Fan, S. Venneti, Y.W. Wan, B.R. Pawel, J. Zhang, L.W. Finley, C. Lu, T. Lindsten, J.R. Cross, G. Qing, Z. Liu, M.C. Simon, J.D. Rabinowitz, C. B. Thompson, Serine catabolism regulates mitochondrial redox control during hypoxia, Cancer Discov. 4 (12) (2014) 1406–1417, https://doi.org/10.1158/2159-8290.Cd-14-0250.

[22] D.J. Kenny, D.R. Plichta, D. Shungin, N. Koppel, A.B. Hall, B. Fu, R.S. Vasan, S.Y. Shaw, H. Vlamakis, E.P. Balskus, R.J. Xavier, Cholesterol metabolism by uncultured human gut bacteria influences host cholesterol level, Cell Host Microbe 28 (2) (2020) 245–257.e6, https://doi.org/10.1016/j.chom.2020.05.013.

[23] D.J. Stekhoven, P. Bühlmann, MissForest–non-parametric missing value imputation for mixed-type data, Bioinformatics 28 (1) (2012) 112–118, https://doi.org/10.1093/bioinformatics/btr597.

[24] M. Asp, S. Giacomello, L. Larsson, C. Wu, D. Fürth, X. Qian, E. Wärdell, J. Custodio, J. Reimegård, F. Salmén, C. Österholm, P.L. Ståhl, E. Sundström, E. Åkesson, O. Bergmann, M. Bienko, A. Månsson-Broberg, M. Nilsson, C. Sylvén, J. Lundeberg, A spatiotemporal organ-wide gene expression and cell atlas of the developing human heart, Cell 179 (7) (2019) 1647–1660.e19, https://doi.org/10.1016/j.cell.2019.11.025.

[25] X. Huang, G. Gan, X. Wang, T. Xu, W. Xie, The HGF-MET axis coordinates liver cancer metabolism and autophagy for chemotherapeutic resistance, Autophagy 15 (7) (2019) 1258–1279, https://doi.org/10.1080/15548627.2019.1580105.

[26] K. Yamamura, T. Uruno, A. Shiraishi, Y. Tanaka, M. Ushijima, T. Nakahara, M. Watanabe, M. Kido-Nakahara, I. Tsuge, M. Furue, Y. Fukui, The transcription factor EPAS1 links DOCK8 deficiency to atopic skin inflammation via IL-31 induction, Nat. Commun. 8 (2017), 13946, https://doi.org/10.1038/ncomms13946.

[27] X.F. Feng, J.J. Hai, Y. Ma, Z.Q. Wang, H.F. Tse, Sudden cardiac death in mainland China: a systematic analysis, Circ Arrhythm Electrophysiol 11 (11) (2018), e006684, https://doi.org/10.1161/circep.118.006684.

[28] A.A. Topjian, A. de Caen, M.S. Wainwright, B.S. Abella, N.S. Abend, D.L. Atkins, M.M. Bembea, E.L. Fink, A.M. Guerguerian, S.E. Haskell, J.H. Kilgannon, J. J. Lasa, M.F. Hazinski, Pediatric post-cardiac arrest care: a scientific statement from the American heart association, Circulation 140 (6) (2019) e194–e233, https://doi.org/10.1161/cir.0000000000000697.

[29] J.T. Niemann, D. Garner, E. Khaleeli, R.J. Lewis, Milrinone facilitates resuscitation from cardiac arrest and attenuates postresuscitation myocardial dysfunction, Circulation 108 (24) (2003) 3031–3035, https://doi.org/10.1161/01.Cir.0000101925.37174.85.

[30] G.D. Perkins, C.W. Callaway, K. Haywood, R.W. Neumar, G. Lilja, M.J. Rowland, K.N. Sawyer, M.B. Skrifvars, J.P. Nolan, Brain injury after cardiac arrest, Lancet 398 (10307) (2021) 1269–1278, https://doi.org/10.1016/s0140-6736(21)00953-3.

[31] G.F. Tomaselli, A.S. Barth, Sudden cardio arrest: oxidative stress irritates the heart, Nat. Med. 16 (6) (2010) 648–649, https://doi.org/10.1038/nm0610-648.

[32] M.A. Smit, I.C. Michelow, J. Glavis-Bloom, V. Wolfman, A.C. Levine, Characteristics and outcomes of pediatric patients with ebola virus disease admitted to treatment units in Liberia and Sierra Leone: a retrospective cohort study, Clin. Infect. Dis. 64 (3) (2017) 243–249, https://doi.org/10.1093/cid/ciw725.

[33] M.A.S. Meyer, S. Wiberg, J. Grand, A.S.P. Meyer, L.E.R. Obling, M. Frydland, J.H. Thomsen, J. Josiassen, J.E. Møller, J. Kjaergaard, C. Hassager, Treatment effects of interleukin-6 receptor antibodies for modulating the systemic inflammatory response after out-of-hospital cardiac arrest (the imica trial): a double-blinded, placebo-controlled, single-center, randomized, clinical trial, Circulation 143 (19) (2021) 1841–1851, https://doi.org/10.1161/circulationaha.120.053318.

[34] C. Hassager, K. Nagao, D. Hildick-Smith, Out-of-hospital cardiac arrest: in-hospital intervention strategies, Lancet 391 (10124) (2018) 989–998, https://doi.org/10.1016/s0140-6736(18)30315-5.

[35] V. Jahandiez, M. Cour, T. Bochaton, M. Abrial, J. Loufouat, A. Gharib, A. Varennes, M. Ovize, L. Argaud, Fast therapeutic hypothermia prevents post-cardiac arrest syndrome through cyclophilin D-mediated mitochondrial permeability transition inhibition, Basic Res. Cardiol. 112 (4) (2017) 35, https://doi.org/10.1007/s00395-017-0624-3.

[36] H.G. Zimmer, The oxidative pentose phosphate pathway in the heart: regulation, physiological significance, and clinical implications, Basic Res. Cardiol. 87 (4) (1992) 303–316, https://doi.org/10.1007/bf00796517.

[37] N.M. Grüning, M. Rinnerthaler, K. Bluemlein, M. Mülleder, M.M. Wamelink, H. Lehrach, C. Jakobs, M. Breitenbach, M. Ralser, Pyruvate kinase triggers a metabolic feedback loop that controls redox metabolism in respiring cells, Cell Metabol. 14 (3) (2011) 415–427, https://doi.org/10.1016/j.cmet.2011.06.017.
[38] S.W. Schaffer, V. Solodushko, D. Kakhniashvili, Beneficial effect of taurine depletion on osmotic sodium and calcium loading during chemical hypoxia, Am. J. Physiol. Cell Physiol. 282 (5) (2002) C1113–C1120, https://doi.org/10.1152/ajpcell.00485.2001.
[39] B.J. Borkowski, Y. Cheema, A.U. Shahbaz, S.K. Bhattacharya, K.T. Weber, Cation dyshomeostasis and cardiomyocyte necrosis: the Fleckenstein hypothesis revisited, Eur. Heart J. 32 (15) (2011) 1846–1853, https://doi.org/10.1093/eurheartj/ehr063.
[40] E.R. Chilvers, C.M. Dixon, Y. Yiangou, S.R. Bloom, P.W. Ind, Effect of peptide histidine valine on cardiovascular and respiratory function in normal subjects, Thorax 43 (10) (1988) 750–755, https://doi.org/10.1136/thx.43.10.750.
[41] K.R. Tuttle, J.E. Milton, D.P. Packard, L.A. Shuler, R.A. Short, Dietary amino acids and blood pressure: a cohort study of patients with cardiovascular disease, Am. J. Kidney Dis. 59 (6) (2012) 803–809, https://doi.org/10.1053/j.ajkd.2011.12.026.
[42] M.I. Flydal, A. Martinez, Phenylalanine hydroxylase: function, structure, and regulation, IUBMB Life 65 (4) (2013) 341–349, https://doi.org/10.1002/iub.1150.
[43] G. Deng, N.D. Vaziri, B. Jabbari, Z. Ni, X.X. Yan, Increased tyrosine nitration of the brain in chronic renal insufficiency: reversal by antioxidant therapy and angiotensin-converting enzyme inhibition, J. Am. Soc. Nephrol. 12 (9) (2001) 1892–1899, https://doi.org/10.1681/asn.V1291892.
[44] V. Jakkamsetti, I. Marin-Valencia, Q. Ma, L.B. Good, T. Terrill, K. Rajasekaran, K. Pichumani, C. Khemtong, M.A. Hooshyar, C. Sundarrajan, M.S. Patel, R. M. Bachoo, C.R. Malloy, J.M. Pascual, Brain metabolism modulates neuronal excitability in a mouse model of pyruvate dehydrogenase deficiency, Sci. Transl. Med. 11 (480) (2019), https://doi.org/10.1126/scitranslmed.aan0457.
[45] A. Falkowska, I. Gutowska, M. Goschorska, P. Nowacki, D. Chlubek, I. Baranowska-Bosiacka, Energy metabolism of the brain, including the cooperation between astrocytes and neurons, especially in the context of glycogen metabolism, Int. J. Mol. Sci. 16 (11) (2015) 25959–25981, https://doi.org/10.3390/ijms161125939.
[46] L.R. Gray, S.C. Tompkins, E.B. Taylor, Regulation of pyruvate metabolism and human disease, Cell. Mol. Life Sci. 71 (14) (2014) 2577–2604, https://doi.org/10.1007/s00018-013-1539-2.
[47] S. Zhang, B.B. Lachance, M.P. Mattson, X. Jia, Glucose metabolic crosstalk and regulation in brain function and diseases, Prog. Neurobiol. 204 (2021), 102089, https://doi.org/10.1016/j.pneurobio.2021.102089.
[48] M. Platten, E.A.A. Nollen, U.F. Röhrig, F. Fallarino, C.A. Opitz, Tryptophan metabolism as a common therapeutic target in cancer, neurodegeneration and beyond, Nat. Rev. Drug Discov. 18 (5) (2019) 379–401, https://doi.org/10.1038/s41573-019-0016-5.
[49] J.K. Sonner, M. Keil, M. Falk-Paulsen, N. Mishra, A. Rehman, M. Kramer, K. Deumelandt, J. Röwe, K. Sanghvi, L. Wolf, A. von Landenberg, H. Wolff, R. Bharti, I. Oezen, T.V. Lanz, F. Wanke, Y. Tang, I. Brandao, S.R. Mohapatra, L. Epping, A. Grill, R. Röth, B. Niesler, S.G. Meuth, C.A. Opitz, J.G. Okun, C. Reinhardt, F. C. Kurschus, W. Wick, H.B. Bode, P. Rosenstiel, M. Platten, Dietary tryptophan links encephalogenicity of autoreactive T cells with gut microbial ecology, Nat. Commun. 10 (1) (2019) 4877, https://doi.org/10.1038/s41467-019-12776-4.
[50] D. Zhang, X. Hu, J. Li, J. Liu, L. Baks-Te Bulte, M. Wiersma, N.U. Malik, D.M.S. van Marion, M. Tolouee, F. Hoogstra-Berends, E.A.H. Lanters, A.M. van Roon, A. A.F. de Vries, D.A. Pijnappels, N.M.S. de Groot, R.H. Henning, B. Brundel, DNA damage-induced PARP1 activation confers cardiomyocyte dysfunction through NAD(+) depletion in experimental atrial fibrillation, Nat. Commun. 10 (1) (2019) 1307, https://doi.org/10.1038/s41467-019-09014-2.
[51] A. Bedalov, J.A. Simon, Neuroscience. NAD to the rescue, Science 305 (5686) (2004) 954–955, https://doi.org/10.1126/science.1102497.
[52] M.S. Bonkowski, D.A. Sinclair, Slowing ageing by design: the rise of NAD(+) and sirtuin-activating compounds, Nat. Rev. Mol. Cell Biol. 17 (11) (2016) 679–690, https://doi.org/10.1038/nrm.2016.93.
[53] A.A. Mangoni, R.N. Rodionov, M. McEvoy, A. Zinellu, C. Carru, S. Sotgia, New horizons in arginine metabolism, ageing and chronic disease states, Age Ageing 48 (6) (2019) 776–782, https://doi.org/10.1093/ageing/afz083.
[54] S. Semsroth, B. Fellner, K. Trescher, O.Y. Bernecker, L. Kalinowski, H. Gasser, S. Hallström, T. Malinski, B.K. Podesser, S-nitroso human serum albumin attenuates ischemia/reperfusion injury after cardioplegic arrest in isolated rabbit hearts, J. Heart Lung Transplant. 24 (12) (2005) 2226–2234, https://doi.org/10.1016/j.healun.2005.08.004.
[55] B.P. Meloni, D. Milani, A.B. Edwards, R.S. Anderton, R.L. O'Hare Doig, M. Fitzgerald, T.N. Palmer, N.W. Knuckey, Neuroprotective peptides fused to arginine-rich cell penetrating peptides: neuroprotective mechanism likely mediated by peptide endocytic properties, Pharmacol. Ther. 153 (2015) 36–54, https://doi.org/10.1016/j.pharmthera.2015.06.002.